High-Density Polyethylene Reinforced With Submicron Titania Particles

Federica Bondioli,[1] **Andrea Dorigato,**[2,3] **Paola Fabbri,**[1,3] **Massimo Messori,**[1,3] **Alessandro Pegoretti**[2,3]
[1] *Dipartimento di Ingegneria dei Materiali e dell'Ambiente, Università di Modena e Reggio Emilia, Via Vignolese 905/A, Modena 41100, Italy*

[2] *Dipartimento di Ingegneria dei Materiali e Tecnologie Industriali, Università di Trento, Via Mesiano 77, Trento 38050, Italy*

[3] *NIPLAB Reference Centre of Italian Interuniversity Consortium on Materials Science and Technology (INSTM), Florence, Italy*

Submicron titania particles were prepared by means of two different synthetic procedures in order to obtain different particle size (diameter ranging from 20 to 350 nm), shapes, and morphologies (amorphous or crystalline). Titania particles were surface modified with octadecylsilane in order to improve their compatibility with respect to polymeric matrices. High-density polyethylene (HDPE)–titania composites were prepared by melt blending by using an internal mixer. The obtained composites were mechanically characterized in quasi static and creep tensile conditions. The presence of submicron titania particles (1 %vol) led to a significant increase of elastic modulus (20–25%) with respect to the unreinforced HDPE together with a slight increase of yield stress and a decrease of ultimate elongation. An interesting reduction for both elastic and viscoelastic creep compliance components was also evidenced. POLYM. ENG. SCI., 48:448–457, 2008.

INTRODUCTION

In conventional microparticle-filled composites, a large amount of fillers (>20 vol%) is generally required to appreciably increase the elastic modulus and reduce the creep compliance of thermoplastic matrices [1]. However, these gains are usually accompanied by severe losses in ductility and toughness. On the other hand, the addition of relatively small amounts (<3 vol%) of inorganic particles such as silica, titania, or calcium carbonate having dimension in the nanometer scale was proven to increase both rigidity and toughness of several different thermoplastics [2]. In fact, both tensile modulus and impact strength improvements were observed by Zhang et al. [3] for high-density polyethylene (HDPE)/silica, Ou et al. [4] for nylon-6/silica, and Xie et al. [5] for poly(vinyl chloride)/$CaCO_3$ nanocomposites. As far as the toughening mechanism is concerned, it is generally believed that cavitation of the polymer matrix surrounding the rigid inorganic particles can promote extensive shear yielding, thus increasing the energy absorbed in highly dissipative phenomena [2, 6]. On the other hand, relatively poor creep resistance is considered as one of the main deficiencies of thermoplastics. In fact, in many intended applications, thermoplastic polymers are often required to sustain long-lasting constant loads with limited deformation. The addition of inorganic nanoparticles was recently proven to be a very promising route to reduce the creep compliance of some thermoplastics. For example, Friedrich and coworkers [7, 8] observed a remarkable reduction of the creep rate of nylon6,6/titania nanocomposites melt compounded using a twin-screw extruder. It is assumed that the nanoparticles may restrict the slippage, reorientation, and motion of polymer chains. In this way, they may influence the stress transfer on a nanoscale, which finally results in the creep resistance improvement.

Among the wide number of commercially available thermoplastic matrices, HDPE is one of the most widely used. In fact, its combination of low cost, high chemical resistance, and well balanced mechanical properties, makes this material ideal for many industrial applications, such as the production of pipes and fittings for the transportation of water or gas under pressure. For this peculiar use, the mechanical response under creep conditions is one of the most important properties to be considered. So far, only limited attempts to improve the creep behavior of HDPE by nanofillers were reported, and all of them are focused on the use of organo-clays. In general, poly-

Correspondence to: Massimo Messori; e-mail: messori.massimo@unimore.it
DOI 10.1002/pen.20973
Published online in Wiley InterScience (www.interscience.wiley.com).

olefins are difficult to be intercalated in the interlayer space of hydrophilic swelling clays without chemical modification of one of the two pristine components. To solve the problem of the lack of interfacial adhesion between apolar polyethylene (PE) and polar layered silicates, the addition of PE grafted with maleic anhydride to the PE matrix was proven to favor the intercalation/exfoliation process, with remarkable improvements of the material stiffness, maintaining the ultimate stress and strain at an acceptable level [9, 10]. Ranade et al. [11] reported that the creep compliance of HDPE blown films can be significantly reduced by the introduction of Cloisite® 15A clay and maleated PE. More recently, Pegoretti et al. [12] confirmed that the creep resistance of HDPE can be enhanced by the introduction of clay, to an extent markedly depending on the viscosity of the polymer matrix, the type of organoclay, and the amount of maleated PE.

In this article, submicron titania particles with different mean diameters (from 350 nm to 30 nm) and morphology were produced by either sol–gel route or hydrothermal crystallization and used to obtain nanocomposites filled at 1 vol% by melt compounding with a HDPE matrix. The effect of both untreated and silane surface-modified particles on the tensile mechanical response of composites were investigated. A particular attention was devoted in understanding their creep behavior.

EXPERIMENTAL SECTION

Preparation of Titania Powders

Titania (TiO_2) particles were prepared by different chemical routes, in order to obtain different morphologies and grain size, whose influence on the mechanical properties of the composites was evaluated.

Monodispersed spherical particles were usually prepared in a 2 l reactor by controlled hydrolysis at room temperature of 1000 ml of tetraethoxy titanium (TEOT, Sigma-Aldrich, Italy) in ethanol (4.8 M) adding a 0.1 M water solution of KCl to control the particles stability [13]. Two different grain size distributions were obtained by changing the salt concentration, through addition of 0.4 or 0.7 ml of KCl solution, respectively. The obtained suspensions were left at room temperature for 240 min.

Different particles morphology was realized by forced hydrolysis in hydrothermal condition starting from a 0.5 M solution of $TiOCl_2$ by applying a microwave thermal treatment [14, 15]. The microwave-assisted syntheses were conducted by using a microwave digestion system (MDS-200, CEM Laboratories, Matthews, NC), working at 2.45 GHz and equipped with both temperature and pressure controls (maximum pressure 14 atm). The reaction vessels were connected to a pressure transducer that monitors and controls the pressure during synthesis. Microwave hydrothermal treatments were conducted at 195°C for 2 h. The time, pressure/temperature, and power were computer controlled. After the synthesis reactions, the obtained suspensions, presenting a pH ranging from 0.9 to 1, were repeatedly washed with bidistilled H_2O to eliminate chloride ions, and successively with NaOH 0.1 N to neutralize the excess of acidity.

Finally, in all cases, the suspensions were washed by repeating centrifugation (4000 rpm for 20 min) and then dried in vacuum a 110°C for 24 h.

Surface Modification of TiO_2 Particles

A typical preparation route was as follows. TiO_2 powders (0.5 g) were placed in a gaschromatograph vial and dried overnight at 120°C in an oven. Ten milliliters of a solution of octadecylsilane ($CH_3(CH_2)_{17}SiH_3$, Sigma-Aldrich, Italy) in toluene were injected into the vial using a syringe (the solutions contained 25 mmol of modifier per square meter of the TiO_2 surface area) [16]. The reaction vessels were left at room temperature for 240 h. The obtained samples were subsequently centrifuged with reagent grade toluene and acetone in order to remove any possible trace of unreacted silane, and then vacuum dried at 110°C over 24 h. A list of the prepared particles is reported in Table 1.

Composites Preparation

Composites were prepared by melt mixing by using a PolyLab Rheomix R600 internal mixer (Thermo Haake GmbH, Germany) equipped with a torque rheometer. Lupolen 5031 L Q 449 (Basell Polyolefins, Italy) having density of 0.952 g/cm^3, melting temperature of 131°C, Melt Flow Rate (MFR) of 6.5 g/10 min (190°C, 2.16 kg), in the physical form of fine powder, was selected as HDPE matrix. Both HDPE and titania particles were dried at 110°C under static vacuum overnight before melt mix-

TABLE 1. Synthesis condition of the obtained particles.

Code	Synthesis
TiO_2-A	Controlled hydrolysis of TEOT, 0.4 ml of 0.1 M KCl aq. slz
M-TiO_2-A	Controlled hydrolysis of TEOT, 0.4 ml of 0.1 M KCl aq. slz, surface modification with $CH_3(CH_2)_{17}SiH_3$
TiO_2-B	Controlled hydrolysis of TEOT, 0.7 ml of 0.1 M KCl aq. slz
M-TiO_2-B	Controlled hydrolysis of TEOT, 0.7 ml of 0.1 M KCl aq. slz, surface modification with $CH_3(CH_2)_{17}SiH_3$
TiO_2-C	Hydrothermal crystallisation of $TiOCl_2$
M-TiO_2-C	Hydrothermal crystallisation of $TiOCl_2$, surface modification with $CH_3(CH_2)_{17}SiH_3$

ing. HDPE (about 40 g) and titania particles (1 vol%) were charged in the internal mixer chamber and dispersed at a temperature of 155°C at a rotors speed of 60 rpm. The mixing time was kept equal to 10 min for all samples.

After melt mixing, sheets having dimensions of 100 × 100 × 1.5 mm^3 were compression molded by using a hot-plate press (Carver, IN) operating at a temperature of 155°C.

Particles Characterization

All the synthesized powders were analyzed with a computer-assisted conventional Bragg-Brentano diffractometer using the Ni-filtered Cu K_α monochromatic radiation (λ = 1.5418 Å) (Philips PW3710, Philips, Netherlands). The X-ray diffraction (XRD) patterns were collected at room temperature in 2θ range of 20–80°, with a scanning rate of 0.005°/s and a step size of 0.02°.

To determine the residual carbon content in the titania particles, elemental analyses were carried out on a Carlo Erba EA 1110 apparatus (Carlo Erba, Italy).

Particle morphology was examined by transmission electron microscopy, JEM 2010 TEM (Jeol, Japan). Specimens were prepared by dispersing the as-obtained powders in distilled water and then placing a drop of suspension on a copper grid covered with a transparent polymer, followed by drying. To estimate the particle size distribution, image analysis was carried on TEM micrographs by using Image Pro Plus 4.5.1 software equipped with the module Materials Pro.

The specific surface area and density of the powders were determined by the B.E.T. method (Gemini 2360 apparatus, Micromeritics, Norcross, GA) and by a picnometer (Accupic 1330 apparatus, Micromeritics, Norcross, GA), respectively.

Particle size was also calculated from the data of specific surface area, using the equation:

$$\phi = \frac{6}{S\rho} \tag{1}$$

where ϕ is the average diameter of the spherical particle, S is the specific surface area of the powder, and ρ is the measured density of titania.

Grafting density (group/nm^2) of the organo modifier was calculated by using the formula: [17]

$$\rho = \frac{6 \times 10^5\,(\%C)}{2400 \times n_C - \mathrm{FW}\ (\%C) \times S(\mathrm{BET})} \tag{2}$$

where FW is the formula weight of the surface modifier (284.6 g/mol), n_C is the number of carbon atoms in the grafted molecule, (%C) is the weight carbon percentage in the sample, and S(BET) is the specific surface area of the bare oxide (m^2/g).

Thermogravimetric/differential thermal analysis (TG/DTA) was carried out on a STA 449C instrument (Netzsch, Germany) at 10°C/min at 20–1000°C temperature range, and the results were used for the determination of the OH groups surface concentration, according to a procedure reported in the literature [18].

Fourier Transform Infrared spectroscopy (FTIR analysis) was performed in the attenuated total reflectance mode with an Avatar 330 spectrometer (Thermo Nicolet, Germany). A minimum of 32 scans with a resolution of 4 cm^{-1} was used.

Composites Characterization

The torque was recorded as a function of mixing time by Lab Rheomix R600 Internal Mixer (Thermo Haake) during melt mixing of HDPE and titania particles, in order to correlate the rheology (melt viscosity) of the composite with particles size and type.

Differential scanning calorimetry was carried out by using a DSC TA 2010 calorimeter (Thermo Analysis, Germany) operating in the following conditions: (i) first heating scan from 30°C to 160°C at 10°C/min, (ii) isothermal at 160°C for 1 min, (iii) cooling scan from 160°C to 30°C at 10°C/min, (iv) isothermal at 30°C for 1 min, (v) second heating scan from 30°C to 160°C at 10°C/min.

The morphology of some composite sample was examined by transmission electron microscopy, JEM 2010 TEM (Jeol, Japan). To prepare specimens for TEM analysis, cryoultramicrotomy was carried out by using a EM UC6 Ultramicrotome (Leica Microsystems GmbH, Germany).

Mechanical Characterization

All mechanical testing was performed with an electromechanical Instron 4502 (Instron, MA) universal tensile testing machine equipped with a 1 kN load cell.

Dumbell specimens (ISO 527 type 1BA, gage length 25 mm, distance between grips 55 mm) were punch-cut from the compression molded sheets and tested under displacement control in uniaxial tensile ramp condition.

The tensile modulus was determined at a crosshead speed of 0.25 mm/min by using a clip-gage extensometer (Instron model 2620-601, gage length 12.5 mm). Because of the large strain involved, the yield and fracture parameters were evaluated at a higher crosshead speed of 50 mm/min, without the extensometer. Three specimens were tested for each sample.

Creep tests were conducted on rectangular strips (length 100 mm, gage length 60 mm) punch-cut from the compression molded sheets. This specimen geometry was selected in order to avoid problems in determining the actual sample gage length, and the deformation was then evaluated by monitoring the crosshead displacement. After a loading ramp at a cross-head speed of 25 mm/min, a constant nominal stress of 10 MPa was applied for

 DOI 10.1002/pen

1 h. Because of the high temperature sensitivity of the creep compliance, the creep tests were carried out at a constant temperature of 30°C in a thermostatic chamber (Instron model 3119).

RESULTS AND DISCUSSION

Particles Preparation and Characterization

Submicron titania particles were produced by either sol–gel route or hydrothermal synthesis in order to evaluate the effect of morphology and crystallinity on the mechanical properties of their composites with a HDPE polymer matrix. As a general rule, in fact, the sol–gel method allows to obtain spherical particles mainly of amorphous nature while the hydrothermal method, especially if supported by microwave heating, enables the crystallization of particles in their crystal habitus.

XRD patterns of synthesized TiO_2 powders are reported in Fig. 1, confirm that all sol–gel samples (TiO_2-A and TiO_2-B) were amorphous while the hydrothermal crystallized titania (TiO_2-C) was mainly composed of rutile phase (80 wt%) phase with a minor amount of anatase (5 wt%) [19].

TEM micrographs revealed that titania particles synthesized by sol–gel method were characterized by a spherical shape and narrow grain size distribution (Fig. 2a and b). Smaller particle size was obtained by introducing a higher concentration of potassium salt (TiO_2-B) according to the results already reported in the literature [14]. Regarding the hydrothermally crystallized powders TiO_2-C (Fig. 2c), the image shows that primary nanocrystals are constituted of faced crystals (average dimension 30 nm) connected tightly to one another. TEM micrograph of M-TiO_2-A (Fig. 2d, chosen as representative) seems to show the presence of an external thin layer with respect to the as prepared TiO_2-A particles (Fig. 2a). This consideration

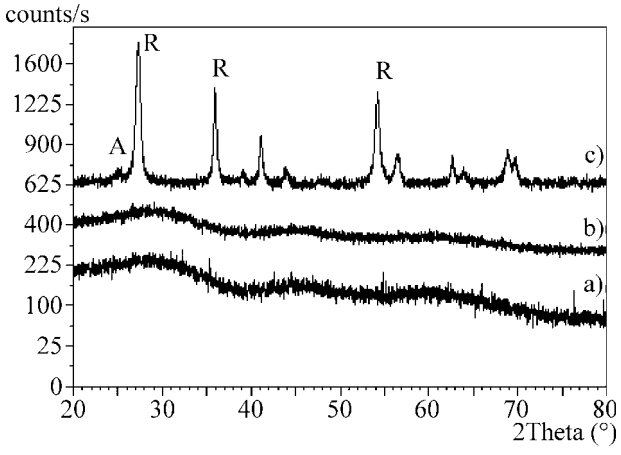

FIG. 1. XRD patterns of titania nanoparticles: (a) TiO_2-A, (b) TiO_2-B, and (c) TiO_2-C (A, anatase phase; R, rutile phase).

was qualitatively supported by EDS analysis (not reported here) which revealed the presence of silicon on the particles surface, indicating the effectiveness of the surface modification treatment with $CH_3(CH_2)_{17}SiH_3$.

As a further support, ATR-IR spectra recorded in the region of CH_2 vibration can be used to investigate the interaction between titania and $CH_3(CH_2)_{17}SiH_3$ as suggested by Helmy and Fadeev [20]. From the spectra reported in Fig. 3, a significant shift of the peaks related to the surface modified titania samples M-TiO_2-A, M-TiO_2-B, and M-TiO_2-C was noted with respect to $CH_3(CH_2)_{17}SiH_3$, consistently with the chemical bonding of octadecylsiloxy groups.

Density, specific surface area, average particles diameter as determined by both TEM images and BET analysis, along with OH concentration and graft density of powders are reported in Table 2.

The elemental analysis carried out on TiO_2-A and TiO_2-B particles showed a significantly high carbon content (6.7 and 9.8%, respectively) and a hydrogen content ranging from 2.8 to 3.4%. These residual presences can be attributed to an incomplete sol–gel reaction of the titania precursor TEOT. A further support to the effectiveness of the surface modification treatment of the particles derived from the significant increase in carbon and hydrogen content (as indicated by elemental analysis) and the decrease of OH groups concentration (as indicated by TG/DTA analysis) in the surface modified particles M-TiO_2-A, M-TiO_2-B, and M-TiO_2-C.

The mean diameters of TiO_2-A, TiO_2-B, and TiO_2-C particles determined from the data of specific surface area B.E.T. are in complete disagreement with those directly determined by TEM (more than one order of magnitude of difference). One possible explanation could be the presence of a porous structure of the particles which in turn underestimates the particle size determined by B.E.T. The significant decrease of specific surface area B.E.T. after surface treatment with $CH_3(CH_2)_{17}SiH_3$, which presumably partially closes the pores, can be taken as a further support to this interpretation. However, this aspect concerning the particle porosity should be investigated in more details.

Composites Characterization

Melt Viscosity. The expected improvement in mechanical properties of composites is usually accompanied by a change in rheological behavior and, in particular, by an increase in melt viscosity. The higher melt viscosity is a disadvantage for processing techniques such as extrusion and injection molding, although it can be beneficial for film extrusion. To gain some information about the melt viscosity of the composites investigated in this study, the torque values were recorded immediately before the end of the run. These data are reported in Table 3 and indicate that the presence of submicron particles slightly modifies the rheology with respect to the pure polymer. The torque

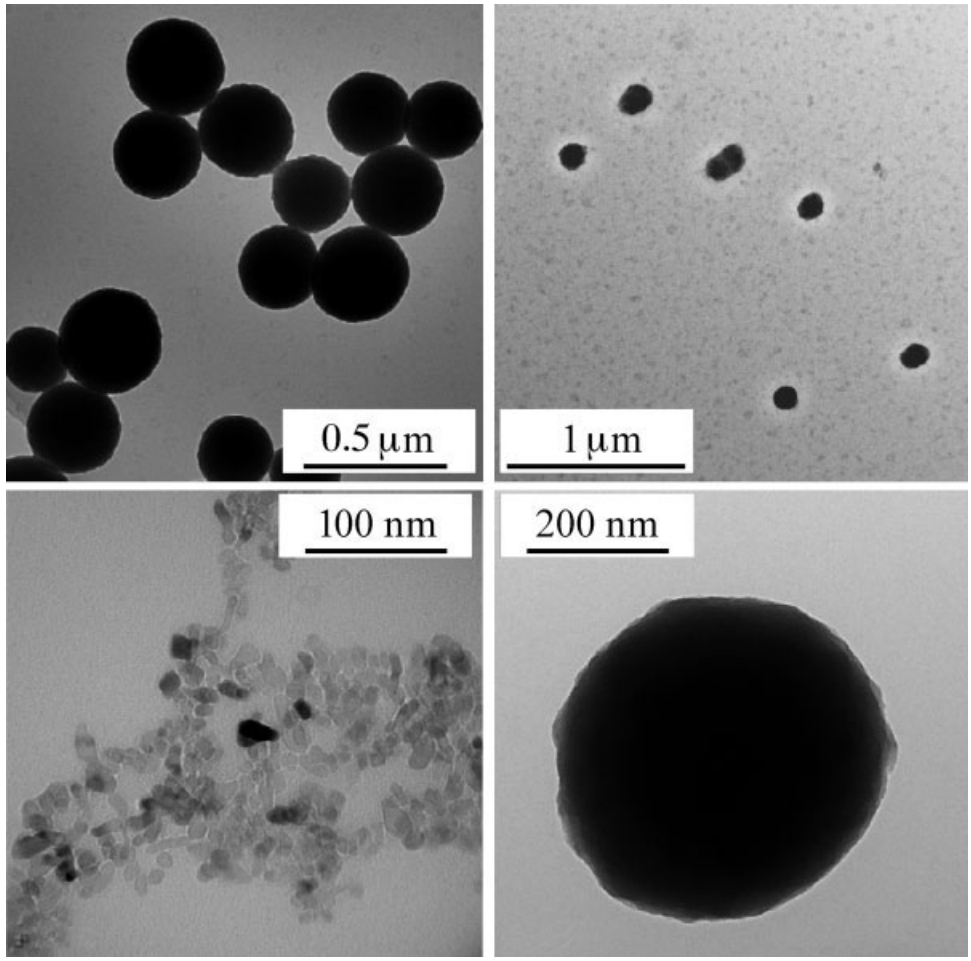

FIG. 2. TEM images of titania particles: (a) TiO_2-A, (b) TiO_2-B, (c) TiO_2-C, and (d) M-TiO_2-A.

measured after 10 min of melt mixing increases from 4.4 N m for pure HDPE to 4.6–4.7 for polymer filled with unmodified particles (TiO_2-A and TiO_2-B) and to 5.0–5.3 for polymer filled with surface modified particles (M-TiO_2-A and M-TiO_2-B). With the exception of the system HDPE/M-TiO_2-C, showing an unexpected decrease of the final torque (4.3 N m), all other composites exhibited an increased melt viscosity due to the presence of a rigid filler, as the general rules for filled polymer melts claim [1]. It is interesting to note that a higher melt viscosity was always obtained in the case of surface modified particles (M-TiO_2-A and M-TiO_2-B) with respect to the unmodified ones (TiO_2-A and TiO_2-B) and this can be considered as a preliminary indication of an improved interaction at the interface between polymer melt and surface modified reinforcing particles.

TEM Analysis. A typical TEM micrograph of an ultramicrotomed composite is reported in Fig. 4 from which the integrity of the particles can be noted. According to the earlier discussed results about melt viscosity, a tightly bound interface between particle and polymer matrix is evident from the reported micrograph.

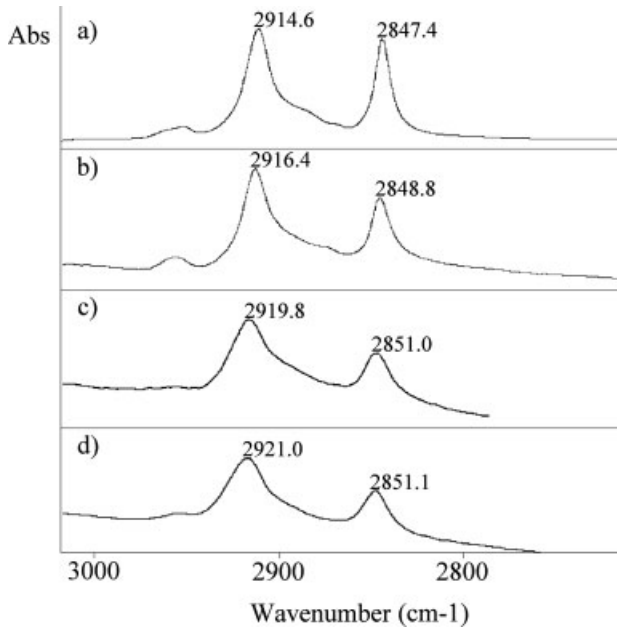

FIG. 3. ATR-IR spectra (CH_2 vibration region) of (a) $C_{18}H_{37}SiH_3$, (b) M-TiO_2-C, (c) M-TiO_2-B, and (d) M-TiO_2-A.

 DOI 10.1002/pen

TABLE 2. Physical properties of the synthesized titania powders.

	TiO_2-A	M-TiO_2-A	TiO_2-B	M-TiO_2-B	TiO_2-C	M-TiO_2-C
Density (g/cm^3)	2.35 ± 0.03	2.80 ± 0.01	2.03 ± 0.01	2.30 ± 0.01	3.71 ± 0.01	3.21 ± 0.01
Surface area by B.E.T. (m^2/g)	237	30	275	154	192	67
Mean diameter by TEM (nm)	350 ± 20	n.d.	150 ± 10	n.d.	30 ± 5	36 ± 5
Mean diameter by B.E.T. (nm)	11	71	11	17	8	7
Elemental analysis N/C/H/S (%wt)	0/6.70/2.76/0	0/9.53/3.30/0	0/9.75/3.39/0	0/12.15/3.62/0	n.d.	0/7.33/1.76/0
OH groups (mmol/g)	7.78	5.16	11.57	9.66	4.44	4.48
Grafting density (groups/nm^2)	n.d.	0.596	n.d.	0.667	n.d.	1.597

DSC Analysis. Melting temperatures and enthalpies (recorded during the first and the second heating scans) and crystallization temperatures and enthalpies (recorded during the first cooling scan) were evaluated from DSC traces (not reported here) and they were substantially the same within the experimental error for all the investigated samples. From this point of view, the presence of 1% by volume of submicron titania particles does not affect the thermal behavior of the composites with respect to the pure polymer.

Mechanical Properties

Constant Rate Tensile Tests. An example of the characteristic instrumented tensile stress–strain curves at low deformation levels is reported in Fig. 5. A pronounced nonlinear behavior can be noticed from very low strain levels. This behavior is quite typically encountered for polymeric materials with a pronounced viscoelastic response, such as many thermoplastics, particularly the partially crystalline ones [21].

As a consequence, according to ISO 527 standard, the elastic modulus E was preferably evaluated as a secant value:

$$E = \frac{\sigma_2 - \sigma_1}{\varepsilon_2 - \varepsilon_1} \tag{3}$$

where, $\varepsilon_1 = 0.05\%$, $\varepsilon_2 = 0.25\%$, while σ_1 and σ_2 are the stress values corresponding to ε_1 and ε_2, respectively.

The resulting tensile modulus values are reported in Table 4.

TABLE 3. Torque values recorded during melt compounding of HDPE/titania composites.

Material code	Torque at 10 min of melt mixing (Nm)
HDPE	4.4
HDPE/TiO_2-A	4.7
HDPE/M-TiO_2-A	5.0
HDPE/TiO_2-B	4.6
HDPE/M-TiO_2-B	5.3
HDPE/M-TiO_2-C	4.3

It is interesting to note that the addition of titania particles, even if at the very low content of 1 vol%, generally causes an improvement of the elastic modulus of the HDPE matrix. For the type A particles (average diameter 350 nm) the modulus is increasing by a similar amount regardless the particle surface treatment. On the other hand, for the type B particles (average diameter 150 nm) the modulus variation is more pronounced when the particles are silane surface modified. The most pronounced stiffening effect is observed for the M-TiO_2-C filled composite, for which an elastic modulus increase of 24% was registered. A stiffening effect can be quantified as $(E_c - E_m)/E_m = \Delta E/E_m$ where E_c and E_m are the composite and matrix moduli, respectively.

This effect can be tentatively modeled by considering the theoretical approaches developed for traditional microcomposites. The static elastic moduli E_c (shear, Young's, or bulk) of a stiff polymer filled with hard, almost spherical particles are well represented by the modified Kerner equation proposed by Lewis and Nielsen [22] in the following form:

$$E_c = E_m \frac{1 + ABV_p}{1 - \Psi BV_p} \tag{4}$$

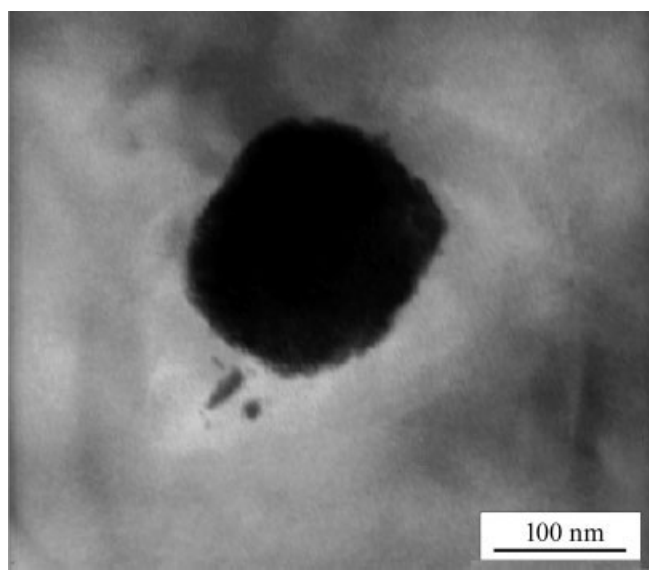

FIG. 4. TEM micrograph of HDPE/M-TiO_2-B.

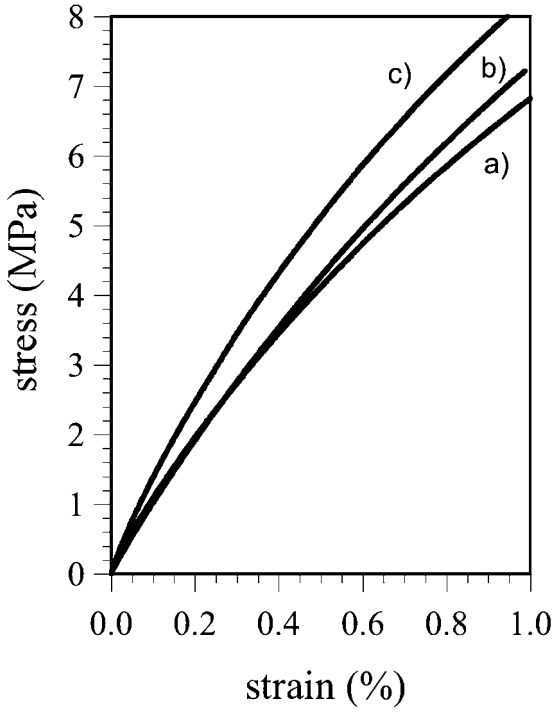

FIG. 5. Small deformations region of the stress–strain curves measured at 0.25 mm/min on (a) HDPE matrix, (b) HDPE/TiO_2-B, and (c) HDPE/M-TiO_2-B nanocomposites.

with

$$A = \frac{7 - 5\nu_m}{8 - 10\nu_m} \tag{5}$$

$$B = \frac{\frac{E_p}{E_m} - 1}{\frac{E_p}{E_m} + A} \tag{6}$$

and

$$\Psi = 1 + \frac{1 - V_{p\text{-max}}}{V_{p\text{-max}}^2} \times V_p \tag{7}$$

where V_p is the particle volume fraction (0.01 in our case), ν_m is the matrix Poisson ratio (0.42 for HDPE [23]), E_p is the modulus of the particles, and $V_{p\text{-max}}$ represents the maximum packing fraction of the filler (0.632 for randomly close packed non-agglomerated spherical particles [1]). It should be noted that, in this model, the Young's modulus does not explicitly depend on the particle size and particle size distribution. Both the parameters and the effect of surface treatment enter into the model only indirectly through the maximum packing fraction $V_{p\text{-max}}$ [24].

The modulus value of the prepared particles is not known since its evaluation is of considerable experimental difficulty. On the other hand, Young's moduli of titania layers with thickness in the range of 280–500 nm were measured by Anderson et al. [25] by means of surface acoustic wave spectroscopy (SAWS). The layers were amorphous or polycrystalline, with densities ranging between 2.9 g/cm^3 and 3.9 g/cm^3 and the modulus resulted to vary between 65 GPa for amorphous films and 147 GPa for polycrystalline ones. The above-mentioned modulus values were therefore adopted for the amorphous (type A and B) and polycrystalline (type C) particles used in this study. The results of the analytical previsions are reported in Table 4 in terms of a theoretical stiffening effect. It is worthnoting that the stiffening effect of the submicron titania particles is in any case much higher than the one theoretically predicted on the basis of the modified Kerner equation. The classical models adopted for microcomposites are not including filler–matrix interactions. On the other hand, these latter phenomena can be important in polymers filled with submicron particles in which the interfacial area is much extended. In fact, modification of the filler–matrix interphase region, such as a reduction [26] or an improvement [27] of the polymer chain mobility was experimentally observed in the case of nanocomposites. These phenomena could therefore account for the observed deviation from classical mechanical models. By introducing a third rigidifying phase of matrix immobilized on the surface of filler particles, Chabert et al. [28] successfully modeled the elastic response of polymer based nanocomposites.

The presence of titania particles also markedly affected the yield and fracture behavior of the HDPE matrix. An example of the characteristic tensile stress–strain curves at high deformation levels is reported in Fig. 6.

It is quite evident that the addition of titania particles slightly improves the yield strength and dramatically reduces the strain at break values. A summary of the results obtained on the investigated composites is reported in Table 5.

Similar effects were recently reported for the same HDPE matrix filled with 2 wt% of organoclay [12]. In polymer/clay nanocomposites, an enhancement of the yield strength, even if small, is generally considered as an indication of a strong filler matrix interaction [11, 29–31].

Tensile Creep Tests. The strain in isothermal tensile creep, ε (t,σ), depending on time t and stress σ, is usually viewed as consisting of three components [32–34]:

TABLE 4. Experimental tensile modulus, E, experimental stiffening effect $(\Delta E/E_m)_{exp}$, and theoretical stiffening effect $(\Delta E/E_m)_{th}$.

Material code	E (MPa)	$(\Delta E/E_m)_{exp}$ (%)	$(\Delta E/E_m)_{th}$ (%)
HDPE	887 ± 7	0	0
HDPE/TiO_2-A	1036 ± 19	16.80	1.26
HDPE/M-TiO_2-A	1022 ± 54	15.22	1.26
HDPE/TiO_2-B	927 ± 52	4.51	1.26
HDPE/M-TiO_2-B	1064 ± 47	19.95	1.26
HDPE/M-TiO_2-C	1100 ± 42	24.01	1.28

DOI 10.1002/pen

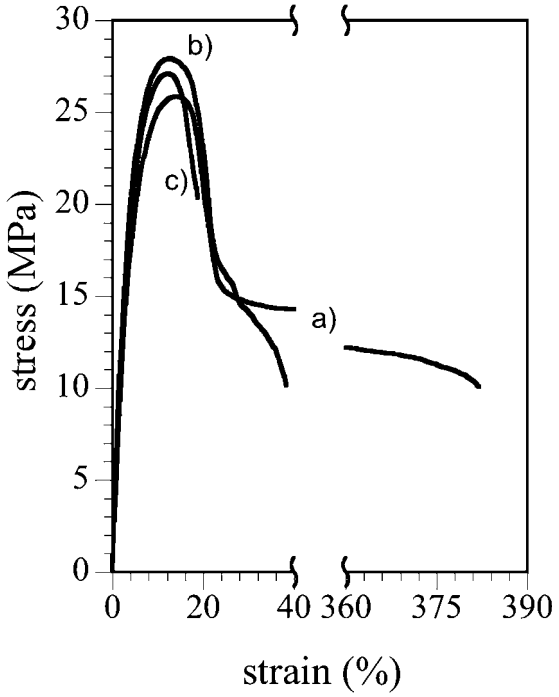

FIG. 6. Stress–strain curves measured at 50 mm/min on (a) HDPE matrix, (b) HDPE/TiO_2-B, and (c) HDPE/M-TiO_2-B nanocomposites.

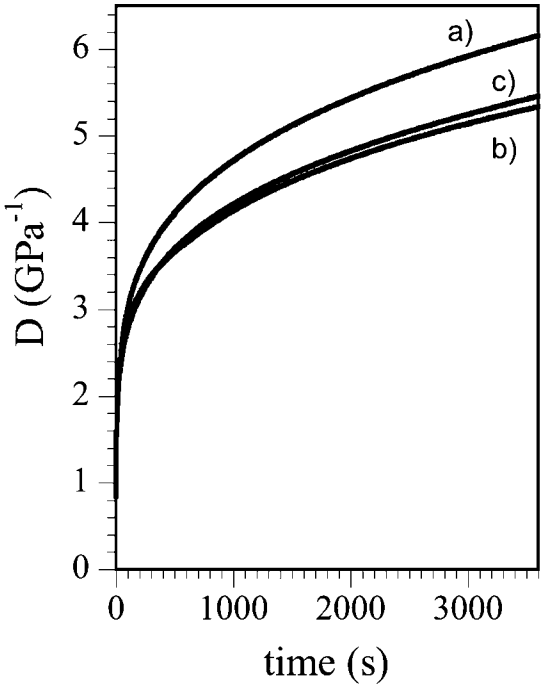

FIG. 7. Creep compliance curves of (a) HDPE matrix, (b) HDPE/TiO_2-B, and (c) HDPE/M-TiO_2-B nanocomposites.

(i) elastic (instantaneous, reversible) $\varepsilon_e(\sigma)$; (ii) viscoelastic (time-dependent, reversible) $\varepsilon_{ve}(t, \sigma)$; (iii) plastic (time-dependent, irreversible) $\varepsilon_p(t, \sigma)$:

$$\varepsilon(t,\sigma) = \varepsilon_e(\sigma) + \varepsilon_{ve}(t,\sigma) + \varepsilon_p(t,\sigma) \tag{8}$$

Linear stress–strain behavior implies that the magnitudes of the three components are linearly proportional to the magnitude of the applied stress, so that a creep compliance $D(t) = \varepsilon(t)/\sigma$ can be defined as a function of time only. If no plastic deformation is produced in the course of the creep test, the tensile compliance $D(t,\sigma) = \varepsilon(t,\sigma)/\sigma$ for the isothermal creep reads

$$D(t) = D_e + D_{ve}(t) \tag{9}$$

In this study, *Eq. 9* was adopted to analyze the experimental data. In fact, all the experiments were performed under the same applied stress in order to avoid nonlinearity effects. Moreover, the specimens recovered their initial length after unloading, thus excluding the presence of plastic deformation.

An example of the creep compliance curves obtained in this study for HDPE-titania composites is reported in Fig. 7.

Submicron titania particles markedly reduces the creep compliance of the HDPE matrix. For both type A and type B particles, a more pronounced creep reduction is obtained when unsized particles are used. A comparison between the creep response of the various composites can be quantified by looking at their creep compliance at a given time. Table 6 summarizes the creep compliance at 2000 s with its elastic and viscoelastic components. It is interesting to note that both elastic and viscoleastic creep compliance components are reduced by the presence of titania nanoparticles, being the type B (smaller diameters) particles slightly more efficient than type A.

A creep rate can be quantified as the time derivative (dD/dt) of the creep compliance curves. As evidenced in Fig. 8, titania particles are also efficient in decreasing the

TABLE 5. Yield strength, σ_y, yield strain, ε_y, stress at break, σ_b, and strain at break, ε_b, of the pure matrix and various composites.

Material code	σ_y (MPa)	ε_y (%)	σ_b (MPa)	ε_b (%)
HDPE	26.3 ± 0.2	13.9 ± 0.2	9.4 ± 0.6	395 ± 59
HDPE/TiO_2-A	27.4 ± 0.6	12.8 ± 0.4	13.8 ± 7.5	30 ± 11
HDPE/M-TiO_2-A	27.8 ± 0.5	12.5 ± 0.2	12.6 ± 2.0	74 ± 32
HDPE/TiO_2-B	27.2 ± 0.9	12.5 ± 0.9	9.8 ± 0.6	40 ± 9
HDPE/M-TiO_2-B	26.4 ± 0.7	11.9 ± 0.9	21.5 ± 1.3	17 ± 2
HDPE/M-TiO_2-C	26.4 ± 0.2	13.3 ± 0.5	18.3 ± 4.6	45 ± 40

TABLE 6. Creep components of HDPE -TiO_2 composites.

Material code	D (t = 2000 s) (GPa^{-1})	D_e (GPa^{-1})	D_{ve} (t = 2000 s) (GPa^{-1})
HDPE	5.434	1.558	3.876
HDPE/TiO_2-A	4.743	1.487	3.256
HDPE/M-TiO_2-A	5.068	1.473	3.595
HDPE/TiO_2-B	4.738	1.322	3.416
HDPE/M-TiO_2-B	4.824	1.404	3.420
HDPE/M-TiO_2-C	5.203	1.442	3.761

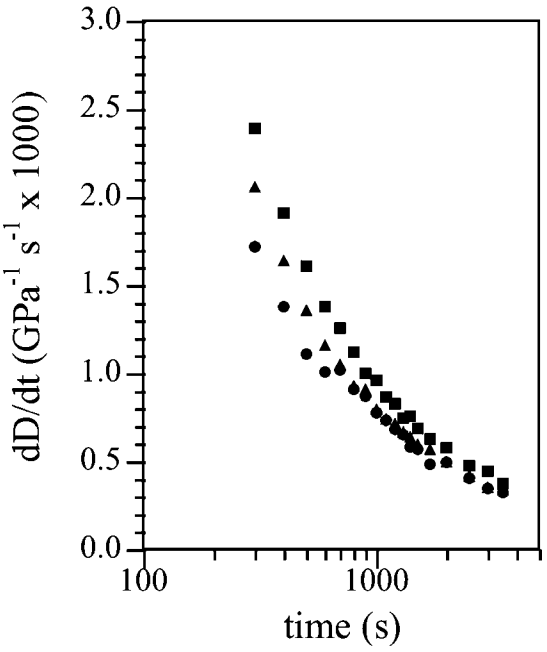

FIG. 8. Creep rate data for ■, HDPE matrix; ●, HDPE/TiO_2-B; and ▲ HDPE/M-TiO_2-B nanocomposites.

creep rate. In particular, it is interesting to observe that the creep rate is more efficiently reduced during the initial stage of the creep experiments, and that the creep rate of composites is converging to that of the HDPE matrix at longer times. This behavior seems to indicate that the long term creep behavior of the investigated composites is a matrix dominated phenomenon, in accordance with the recent observation of Siengchin and Karger-Kocsis [35] on the creep behavior of polystyrene/fluorohectorite micro and nanocomposites.

CONCLUSIONS

In this work, submicron titania particles with different particle size, shape, and morphology were easily prepared by controlled hydrolysis of tetraethoxy titanium or by microwave-assisted hydrothermal crystallization of $TiOCl_2$. The average diameter was varied from 30 nm to 350 nm and the particles were either amorphous or crystalline (with the rutile phase mainly present). Titania particles were successfully surface modified with octadecylsilane in order to improve their compatibility with respect to HDPE matrices. The incorporation of 1 vol% titania particles into HDPE led to the formation of composite materials with improved elastic modulus. The presence of titania particles also markedly affected the yield and fracture behavior of the HDPE matrix and in particular the addition of this kind of reinforcement slightly improved the yield strength together with a dramatic reduction of the strain at break. Regarding the creep properties, a marked reduction of the creep compliance was noted for all HDPE/titania composites with respect to the pure HDPE. Both elastic and viscoleastic creep compliance components were reduced by the presence of titania particles, being the smaller diameter nanoparticles slightly more efficient than the larger ones.

ACKNOWLEDGMENTS

Ms. Ilaria Puccini is gratefully acknowledged for her support to experimental work.

REFERENCES

1. L.E. Nielsen and R.F. Landel, *Mechanical Properties of Polymers and Composites*, Marcel Dekker, New York (1994).
2. S.C. Tjong, *Mater. Sci. Eng. R*, **53**, 73 (2006).
3. M.Q. Zhang, M.Z. Rong, H.B. Zhang, and K. Friedrich, *Polym. Eng. Sci.*, **43**, 490 (2003).
4. Y.C. Ou, F. Yang, and Z.Z. Yu, *J. Polym. Sci. Part B: Polym. Phys.*, **36**, 789 (1998).
5. X.L. Xie, Q.X. Liu, R.K.Y. Li, X.P. Zhou, Q.X. Zhang, Z.Z. Yu, and Y.W. Mai, *Polymer*, **45**, 6665 (2004).
6. A. Lazzeri, S.M. Zebarjad, M. Pracella, K. Cavalier, and R. Rosa, *Polymer*, **46**, 827 (2005).
7. J.L. Yang, Z. Zhang, A.K. Schlarb, and K. Friedrich, *Polymer*, **47**, 6745 (2006).
8. Z. Zhang, J.L. Yang, and K. Friedrich, *Polymer*, **45**, 3481 (2004).
9. K. Chrissopoulou, I. Altintzi, S.H. Anastasiadis, E.P. Giannelis, M. Pitsikalis, N. Hadjichristidis, and N. Theophilou, *Polymer*, **46**, 12440 (2005).
10. M.A. Osman, J.E.P. Rupp, and U.W. Suter, *Polymer*, **46**, 8202 (2005).
11. A. Ranade, K. Nayak, D. Fairbrother, and N.A. D'Souza, *Polymer*, **46**, 7323 (2005).
12. A. Pegoretti, A. Dorigato, and A. Penati, *Express Polym. Lett.*, **1**, 123 (2007).
13. S. Eiden-Assmann, J. Widoniak, and G. Maret, *Chem. Mater.*, **16**, 6 (2004).
14. A.B. Corradi, F. Bondioli, B. Focher, A.M. Ferrari, C. Grippo, E. Mariani, and C. Villa, *J. Am. Ceram. Soc.*, **88**, 2639 (2005).
15. S. Komarneni, R.K. Rajha, and H. Katsuki, *Mater. Chem. Phys.*, **61**, 50 (1999).
16. A.Y. Fadeev, R. Helmy, and S. Marcinko, *Langmuir*, **18**, 7521 (2002).
17. S. Marcinko and A.Y. Fadeev, *Langmuir*, **20**, 2270 (2004).
18. R.F. de Farias and C. Airoldi, *J. Therm. Anal. Calorim.*, **53**, 751 (1998).
19. A. Bonamartini Corradi, F. Bondioli, A.M. Ferrari, and M. Romagnoli, submitted for publication.
20. R. Helmy and A.Y. Fadeev, *Langmuir*, **18**, 8924 (2002).
21. J. Kolarik and A. Pegoretti, *Polymer*, **47**, 346 (2006).
22. T.B. Lewis and L.E. Nielsen, *J. Appl. Polym. Sci.*, **14**, 1449 (1970).
23. Z.M. Li, M.B. Yang, R. Huang, and J.M. Feng, *J. Elastom. Plast.*, **35**, 15 (2003).

 DOI 10.1002/pen

24. H.H. Kausch, P. Beguelin, and M. Fischer, *Mech. Compos. Mater.*, **36**, 177 (2000).
25. O. Anderson, C.R. Ottermann, R. Kuschnereit, P. Hess, and K. Bange, *Fresenius J. Anal. Chem.*, **358**, 315 (1997).
26. D. Ciprari, K. Jacob, and R. Tannenbaum, *Macromolecules*, **39**, 6565 (2006).
27. H.E. Miltner, H. Rahier, A. Pozsgay, B. Pukanszky, and B. Van Mele, *Compos. Interface.*, **12**, 787 (2005).
28. E. Chabert, R. Dendievel, C. Gauthier, and J.Y. Cavaille, *Compos. Sci. Technol.*, **64**, 309 (2004).
29. S. Hotta and D.R. Paul, *Polymer*, **45**, 7639 (2004).
30. J. Morawiec, A. Pawlak, M. Slouf, A. Galeski, E. Piorkowska, and N. Krasnikowa, *Eur. Polym. J.*, **41**, 1115 (2005).
31. M. Tanniru, Q. Yuan, and R.D.K. Misra, *Polymer*, **47**, 2133 (2006).
32. R.J. Crawford, *Plastics Engineering*, Butterworth-Heinemann, Oxford, UK (1998).
33. R.S. Lakes, *Viscoelastic Solids*, CRC Press, Boca Raton (1999).
34. I.M. Ward and D.W. Hadley, *An Introduction to the Mechanical Properties of Solid Polymers*, Wiley, Chichester (1993).
35. S. Siengchin and J. Karger-Kocsis, *Macromol. Rapid Commun.*, **27**, 2090 (2006).